CHEMISTRY OF MATERIALS

ARTICLE

pubs.acs.org/cm

Controlled Electrochemical Formation of $Ge_xSb_yTe_z$ using Atomic Layer Deposition (ALD)

Xuehai Liang, Nagarajan Jayaraju, Chandru Thambidurai, Qinghui Zhang, and John L. Stickney*

Department of Chemistry, The University of Georgia, Athens, Georgia 30602, United States

ABSTRACT: This paper describes a systematic study of the deposition of a phase change material, $Ge_xSb_yTe_z$, using electrochemical atomic layer deposition (E-ALD). Cyclic voltammetry in aqueous solutions was used to investigate the deposition of atomic layers of Ge, Sb and Te. That data was used to develop initial E-ALD cycle conditions to form the binaries: Sb_xTe_y and Ge_xTe_y. Films of the ternary material $Ge_xSb_yTe_z$, were then deposited with a wide range of compositions by alternating the binary cycles in various combinations. Conformal nanofilms were formed that exhibited good crystallinity.

KEYWORDS: ALD, E-ALD, phase change memory, UPD, electrodeposition

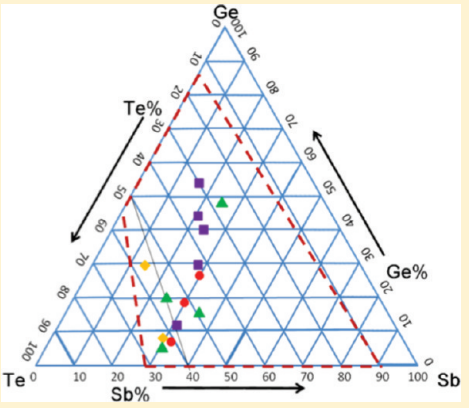

INTRODUCTION

Phase change materials have at least two different solid phases, normally one amorphous and one crystalline, exhibiting distinct properties, i.e., optical and/or resistance disparities, due to the differences in structure.[1−3] Application of phase change materials for optical storage utilizing differences in optical constants, have been successfully commercialized.[1] Researchers are now focusing on the use of phase change materials to make nonvolatile electronic storage, as some phase change materials show differences in resistance and "threshold point", in addition to differences in optical properties.[1,4−6] When the potential applied to an amorphous phase change material is higher than the threshold point, the current increases dramatically, generating heat and so a phase change. Phase change materials may facilitate the formation of nonvolatile electronic storage as a possible replacement in flash drives, or in applications in dynamic random access memory and reconfigurable logic (cognitive computing).[2,7] Among those materials, $Ge_xSb_yTe_z$ is promising as it has shown large optical and resistance differences between amorphous and crystalline states, fast phase transition speed, good scalability, and high stability.[3,8] Its properties can be modified by adjusting the composition for different applications.[9−12] For example, increases in Ge result in increased stability, resistance and crystallization temperature.

Sputtering has been the preferred deposition method for fabricating optical storage, as it is a well established deposition method with good scalability, reproducibility, and uniformity. It is also capable of high rates and good composition control. However, sputtering becomes limited in the formation of electronic storage, where the material must be deposited in trenches or vias with high aspect ratios. Sputtering is line of sight, which presents problems for the formation of conformal deposits. To improve trench filling, other deposition methods have been proposed and studied, e.g., metal organic chemical vapor deposition (MOCVD),[13−15] solution phase deposition[16] and electrodeposition.[17,18]

Electrodeposition has excellent trenching filling capability, and is typically operated near room temperature and ambient pressure. In addition, electrodeposition is compatible with patterned resist technology, and therefore may be easily scaled.[2] Two electrodeposition methodologies with possible applications here are electrochemical codeposition[19−22] and electrochemical atomic layer deposition (E-ALD).[23,24] Co-deposition is known to be a cost-effective methodology, though E-ALD has more control over the deposition process and film composition. Films made by E-ALD tend to have crystalline structures, whereas films formed by codeposition do not.[17,19,25] Better crystallinity can help minimize or eliminate defects in the films, resulting from volume shrinkage and void formation.[18] In addition, E-ALD is well suited for conformal deposition. In the development of $Ge_xSb_yTe_z$ for electronic storage applications, workers have, in order to lower the programming current, designed cells with specific patterns,[26,27] which will require conformal deposition.

E-ALD involves the sequential electrodeposition of atomic layers of elements to form nanofilms of a material. Note that "atomic layer" referrers to an elemental layer no more than an atom thick, but of an undefined coverage. E-ALD is based on the use of electrochemical surface limited reactions, frequently referred to as underpotential deposition (UPD). UPD is a phenomenon where an atomic layer of one element deposits on a second at a potential prior to (under) that needed to deposit

Received: September 16, 2010
Revised: February 17, 2011
Published: March 11, 2011

the bulk element. UPD is a manifestation of the negative free energy of formation for a surface compound or alloy.[23,28−31] E-ALD results in atomic layer control over the formation of nanofilms deposits.

IBM has investigated both electrochemical codeposition and E-ALD for the formation of $Ge_xSb_yTe_z$.[18,32] In their codeposition patent, they demonstrated the capability for codepositing Ge, Sb and Te, onto patterned structures, on different substrates. They claim that they were able to synthesize $Ge_xSb_yTe_z$ within the ranges: $0 < x < 0.4$, $0 < y < 0.8$, and $0 < z < 0.8$. The samples shown in their patent were $Ge_8Sb_{62}Te_{30}$, $Ge_{11}Sb_{59}Te_{30}$, and $Ge_{12}Sb_{60}Te_{28}$, all rich in Sb, with little variation in Ge and Te percentages. In their E-ALD patent application, they described a detailed study of Sb_2Te_3, and stated that Ge does not deposit on the Te covered substrate.[32] They suggested that $Ge_xSb_yTe_z$ could be deposited by forming a sequence of elemental films: Te, followed by Sb, followed by Ge. No data consistent with that process were shown.

The purpose of this study was to fill current gaps in the E-ALD chemistry needed to electrodeposit $Ge_xSb_yTe_z$. The ability to form $Ge_xSb_yTe_z$ in aqueous solution, via electrodeposition, should facilitate applications of $Ge_xSb_yTe_z$, and so development of nonvolatile phase change memory. The report further demonstrates the potential of E-ALD as a technique for the fabricating electronic storage, given its ability to form conformal deposits, while maintaining control over composition and improving crystallinity. This report describes how the composition of $Ge_xSb_yTe_z$ can be manipulated with the E-ALD cycle and a superlattice program based on the binary compounds: Sb_xTe_y and Ge_xTe_y. A number of deposits demonstrating control over the $Ge_xSb_yTe_z$ composition are reported.

EXPERIMENTAL SECTION

The E-ALD hardware has been described previously[33] (Electrochemical ALD L.C., Athens GA), and consisted of pumps, valves, an electrochemical flow cell and a potentiostat, all computer-controlled via a specialized program. Solutions, valves and tubing were confined inside a nitrogen purged Plexiglas box, to exclude oxygen. The flow cell was similar to that described previously,[33] though the auxiliary electrode was a Au wire, rather than ITO. The reference electrode was Ag/AgCl (3 M NaCl) (Bioanalytical systems, inc., West Lafayette, IN). Substrates were 300 nm thick gold films formed on a 10 nm adhesion layer of Ti, on a glass slide. The deposits were annealed at 400 °C for 12 h, under a a 1×10^{-6} Torr vacuum. The resulting films displayed a predominant [111] habit.

Solution flow rates were 18 mL/min. Cyclic voltammetry of the gold substrates in 0.1 M H_2SO_4 was used to clean the substrates, and to check cleanliness before each experiment. The solutions were formed using high purity oxides, which hydrolyzed in water (eqs 1-3): 5 mM $HGeO_3^-$ (pH 9.4), 0.2 mM TeO_3^{2-} (pH 9.4) and 0.05 mM SbO_2^- (pH 9.4).

The following are the hydrolysis reactions at pH 9.4

$$GeO_2 + OH^- = HGeO_3^- \quad (1)$$

$$Sb_2O_3 + 2OH^- = 2SbO_2^- + H_2O \quad (2)$$

$$TeO_2 + 2OH^- = TeO_3^{2-} + H_2O \quad (3)$$

All solutions contained 0.5 M Na_2SO_4 as a supporting electrolyte and 50 mM $Na_2B_2O_4$ as a buffer. The blank solution contained only the electrolyte and buffer. Water used for solutions was supplied from a Nanopure water filtration system (Barnstead, Dubuque, IA). Chemicals were reagent grade or better. All solutions were purged with nitrogen before and during experiments, to minimize oxygen levels in the solutions.

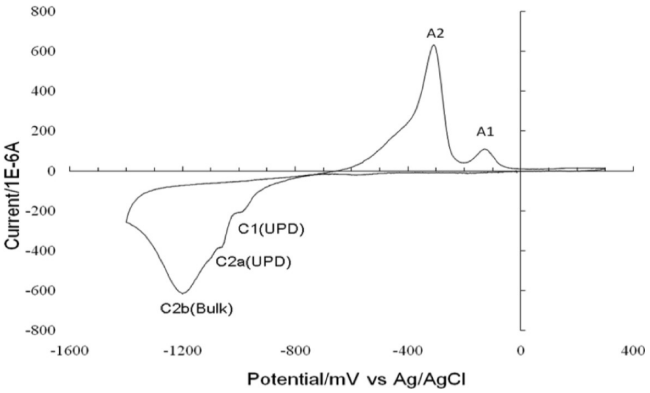

Figure 1. Cyclic voltammogram of Au in a solution containing: 0.5 M Na_2SO_4 + 50 mM $Na_2B_2O_4$ + 5 mM $HGeO_3^-$, at pH 9.40. The electrode area was 3.3 cm^2 and the scan rate was 10 mV/s).

A Scintag PAD-V diffractometer, with Cu Kα radiation (λ = 1.5418 Å), was used to obtain glancing-angle XRD patterns. Electron probe microanalysis (EPMA) was run on a Joel 8600 wavelength dispersive scanning electron microprobe for composition analysis. Annealing was done in a quartz tube, in a nitrogen atmosphere, using a Lindberg Blue M tube furnace. Atomic force microscopy (Molecular Imaging picoscan) was used under intermittent contact mode to characterize deposit morphology. Images were processed and analyzed with WSXM software. A Jenavert optical metallographic microscope was used to initially check homogeneity and morphology.

RESULTS AND DISCUSSION

Elements. Figure 1 shows a cyclic voltammogram (CV) for a Au substrate in the pH 9.4 $HGeO_3^-$ solution. A previous study, by this group, concerned Ge deposition on Au from aqueous solutions, and showed a strong dependence on pH. pH 9.4 (Figure 1) resulted in the most deposition and the best defined CV peaks.[23] The 10 mV/s scan started negatively from 300 mV, and displayed three reduction peak features (C1, C2a, and C2b) prior to hydrogen evolution. Two primary oxidation features (A1 and A2), were evident in the subsequent positive going scan. Peak C1 (eq 4) corresponds to the formation of a Au(111)(3×3)-GeOH surface structure, at 4/9 ML coverage, while C2a (eq 5) corresponds to an increase in coverage and transformation to a hydride structure displaying a moiré pattern.[23] Both C1 and C2a have surface limited character. The third peak, C2b, corresponds to some bulk Ge deposition. The left oxidation peak, A2, was oxidation of bulk Ge, leaving the (3×3)-GeOH structure, while A1 is the oxidation of the (3×3)-GeOH structure to soluble $HGeO_3^-$. From those results, it was concluded that an atomic layer of Ge might be deposited using potentials between −800 and −1070 mV, in surface limited reactions.[23] The amount of Ge deposited was adjustable, the coverage increasing the more negative the potential.

$$HGeO_3^- + 3e^- + 2H_2O = GeOH(ad) + 4OH^- \quad (4)$$

$$GeOH(ad) + 2e^- + H_2O = GeH(ad) + 2OH^- \quad (5)$$

An alternative Ge atomic layer deposition strategy is to first deposit a Ge atomic layer using an overpotential, producing the atomic layer with a small amount of bulk Ge. The bulk Ge could

dx.doi.org/10.1021/cm102672j |Chem. Mater. 2011, 23, 1742–1752

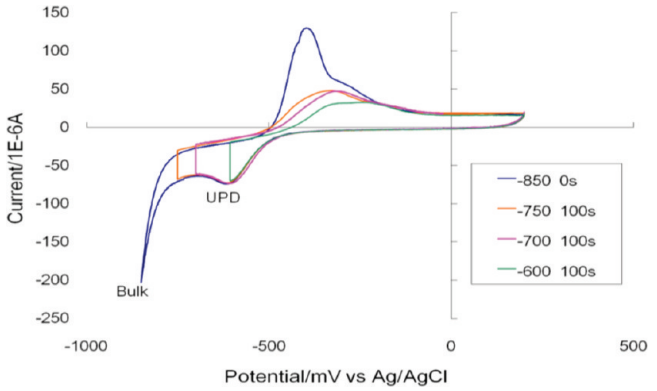

Figure 2. CVs of Au in a solution containing 0.5 M Na_2SO_4 + 50 mM $Na_2B_2O_4$ + 0.05 mM SbO_2^-, at pH 9.4. The electrode area was 3.3 cm^2, whereas the scan rate was 10 mV/s.

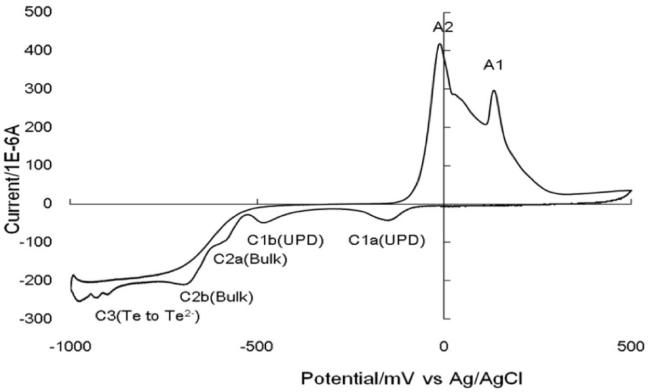

Figure 3. Cyclic voltammogram of Au in a solution containing 0.5 M Na_2SO_4 + 50 mM $Na_2B_2O_4$ + 0.2 mM TeO_3^{2-}, pH 9.4. The electrode area was 3.3 cm^2, whereas the scan rate was 10 mV/s.

then be oxidatively stripped at a potential just positive of the formal potential Ge oxidation. In that way, only an atomic layer of a Ge species, Ge UPD, would be left. As can be seen in Figure 1, bulk oxidation (peak A2) and UPD oxidation (peak A1) are resolved, allowing bulk oxidation without stripping the UPD. The resulting coverage can be adjusted using the potential selected for oxidative stripping. In general, direct UPD is preferable, unless the kinetics are slow and require an overpotential. The measured formal potential under the stated conditions for bulk Ge deposition was −1.1 V (vs Ag/AgCl).

Figure 2 shows window opening CVs for a Au substrate in the pH 9.4 SbO_2^- solution: the substrate was cycled to increasingly negative potentials. All CVs started negative from 200 mV at 10 mV/s. In addition, the CVs were held fixed at the negative potential limits for 100 s, except for the scan reversed at −850 mV. The window opening confirmed that the reduction peak marked UPD was surface limited, even though it was formed at a slight overpotential.[34−36] Between −400 and −750 mV, holding for 100 or 200 s resulted in essentially the same coverage, determined from the resulting oxidation charges, further indicating the surface limited nature of the reaction. However, the coverage did increase with increasing time held at −800 mV, suggesting bulk Sb formation. Equation 6 describes Sb reduction, for which a formal potential of −0.75 V (vs Ag/AgCl) was measured for the stated conditions. Bulk and UPD Sb oxidation overlap in Figure 2, suggesting direct reductive UPD at a potential between −400 and −750 mV should work better then oxidative stripping step.

$$SbO_2^- + 3e^- + 2H_2O = Sb + 4OH^- \quad (6)$$

Figure 3 shows a CV for Au in the pH 9.4 TeO_3^{2-} solution, starting negative from 500 mV. C1a and C1b have been previously reported as surface limited features, similar to UPD, though formed at overpotentials.[33,37−40] C2a and C2b are associated with bulk Te deposition (eq 7), and C3 is reduction of bulk Te to Te^{2-} (eq 8). The measured potential for bulk Te formation, under the conditions stated here, was −0.53 V (vs Ag/AgCl). No formal potential can be stated, based on these studies, for eq 7 due to the slow kinetics. The oxidation peak A2 in the subsequent positive going scan corresponds to bulk Te oxidation to TeO_3^{2-}, and A1 corresponds to oxidation of a surface limited Te atomic layer.[28,40] Deposition at potentials from C1a to C2b resulted in different Te atomic layer coverages. Bulk Te deposition began near C2a, though only slowly, reaching a maximum at C2b. Further reduction, C3, forms Te^{2-} from bulk Te and TeO_3^{2-} impinging on the surface. The last Te atomic layer is difficult to reductively strip as Te^{2-}, because of the stability of Au−Te bonding.

$$TeO_3^{2-} + 4e^- + 3H_2O = Te + 6OH^- \quad (7)$$

$$Te + 2e^- = Te^{2-} \quad (8)$$

There are a couple electrochemical methodologies for the formation of a Te atomic layer.[17,28] Deposition at a potential in the surface limited region (C1b to C2a) should form an atomic layer, though with a trace of bulk Te. The actual bulk potential for eq 7 is believed, by these authors, to be near −150 mV, though due to the slow kinetics, little bulk Te is formed until C2a. If other component elements are stable at positive potentials, oxidative stripping of the bulk Te can be performed between A2 and A1, leaving an atomic layer. If other elements present are not stable at such positive potentials, reductive stripping can be used, where the TeO_3^{2-} solution is exchanged for a blank. A negative potential is applied to reductively strip bulk Te as Te^{2-}, leaving only a Te atomic layer. This third Te atomic layer formation method was used in the present studies, to avoid oxidation of Sb and Ge during Te deposition, and to avoid formation of even a trace of bulk Te.

Binary Systems. *Sb_xTe_y.* Stoichiometric electrodeposition of Sb_2Te_3 has been formed using codeposition, atom by atom codeposition and E-ALD.[19,22,25,41,42] Venkatasamy used E-ALD to form crystalline deposits that filled high-aspect-ratio trenches.[17] Yang also reported the E-ALD formation of crystalline Sb_2Te_3 on Au and Pt substrates.[41,43] The present report describes approaches for controlling the composition of Sb_xTe_y formed using E-ALD. The starting points were the conditions determined from the CVs described above.

Sb UPD was performed between −400 and −750 mV, whereas Te atomic layers were formed at an overpotential, producing a surface limited Te layer with a little bulk, as described above, with the bulk removed by reductive stripping at a negative potential in blank. More Te deposition resulted from the use of more negative Te deposition potentials, which then required more bulk to be removed to form an atomic layer. Te atomic layer coverages proved sensitive to the potential used for reductively stripping bulk Te. The more negative the stripping potential, the lower the resulting Te atomic layer coverage.

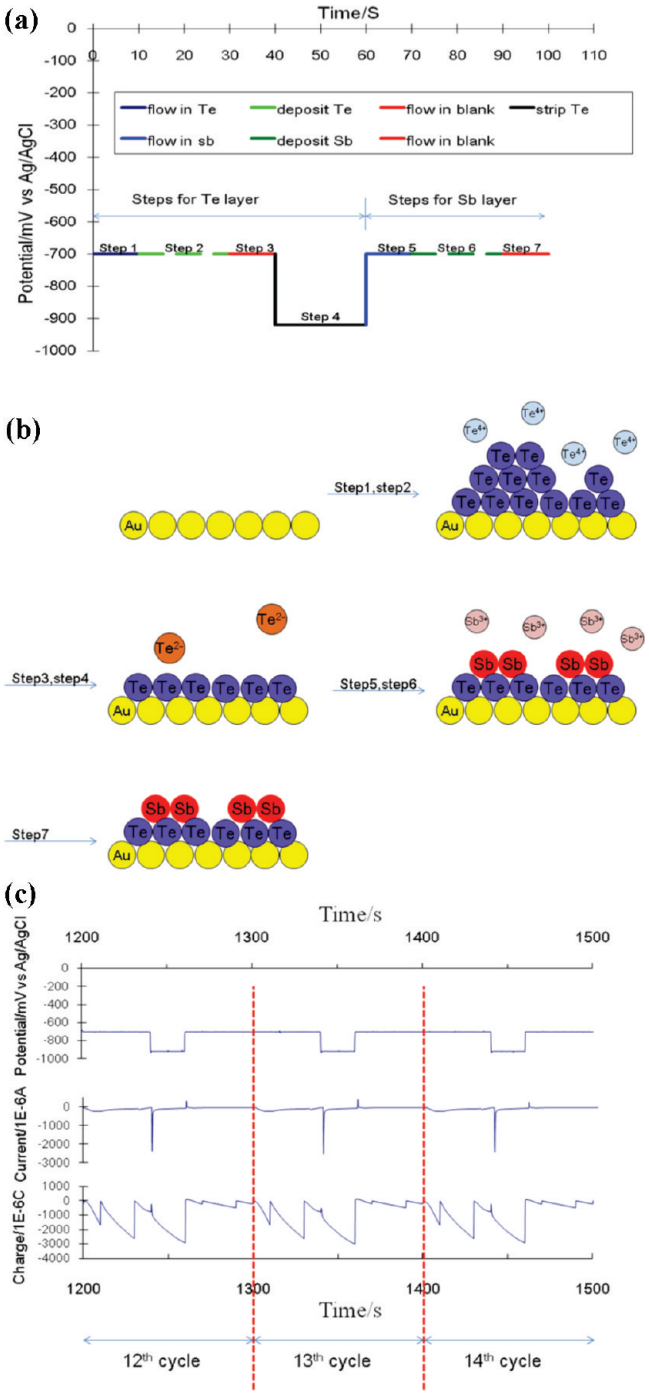

Figure 4. (a) An example of a Sb_xTe_y deposition cycle. Solid lines indicate solution flowing and dashed lines indicate stagnant solutions. (b) Deposition cycle scheme for Sb_xTe_y binary layer deposition. (c) Deposition potential, current, and charge for three consecutive Sb_xTe_y deposition cycles.

Figure 4a is a diagram for a Sb_xTe_y E-ALD cycle, whereas Figure 4b is a corresponding scheme. Solid lines in Figure 4a indicate when a solution flowed, whereas dashed lines (Figure 4a) indicate stagnant solution. Step 1 was introduction of the TeO_3^{2-} solution for 10 s at −700 mV. In step 2, the solution was held at −700 mV for 20 s, no flow, for Te deposition. In step 3, the blank was flushed in at −700 mV for

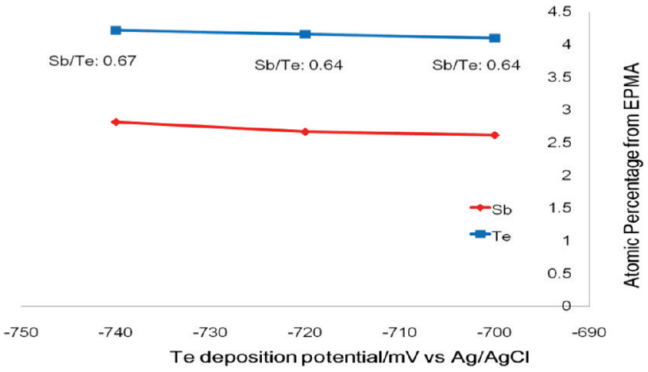

Figure 5. Sb_xTe_y composition as a function of Te deposition potential.

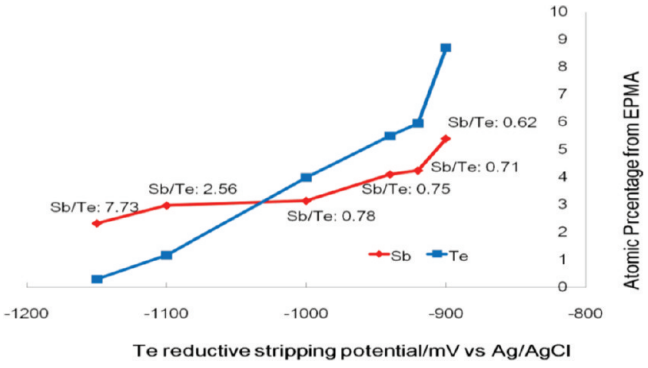

Figure 6. Sb_xTe_y composition as a function of Te reductive stripping potential.

10 s to remove extra TeO_3^{2-} ions. In Step 4 the potential was stepped to −920 mV, to convert bulk Te to Te^{2-}, with the blank flowing. In step 5, the SbO_2^- solution was flowed for 10 s at −700 mV (step 5), followed by step 6, where the potential was held at −700 mV for 20 s more, without flowing, to deposit a Sb atomic layer. Step 7 was a blank flush to remove SbO_2^-. Deposition times can be reduced significantly with faster pumps. Figure 4c displays potentials, currents, and charges for three consecutive cycles, showing reproducibility.

Each cycle can be broken into three sections: Te deposition, bulk Te stripping, and Sb UPD. Te controlling the Sb_xTe_y composition.

Figure 5 shows a nearly constant Sb/Te ratio for the short-range of potentials used for Te deposition, between −700 and −740 mV. Steps 4 through 7 were kept constant (Te stripping at −920 mV and Sb deposition at −700 mV), only steps 1−3 were modified. Deposits were formed using 50 cycles.

In contrast to Figure 5, Figure 6 displays significant changes in deposit composition and elemental coverages as a function of the Te reductive stripping potential (Step 4). As in Figure 3, reduction of Te to Te^{2-} became significant below −900 mV, with Te deposition at −700 mV and Sb deposition at −720 mV. The presence of excess Te was visible as 3D black crystal clusters, using optical microscopy. Below −900 mV, bulk Te was removed, leaving only a Te atomic layer each cycle, and facilitating conformal growth. No roughening was observed using optical or atomic force microscopy. At the more negative stripping potentials, only strongly bound Te atoms remained, most likely those highly coordinated to Sb. The Te atomic % from EPMA (a rough indication of the relative coverage of Te in the deposit) dropped

dx.doi.org/10.1021/cm102672j |*Chem. Mater.* 2011, 23, 1742–1752

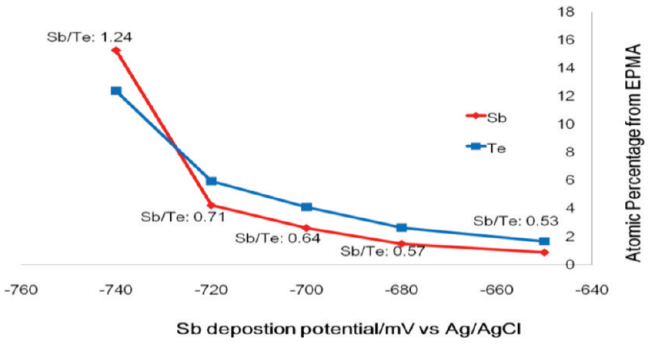

Figure 7. Sb_xTe_y composition as a function of Sb deposition potential.

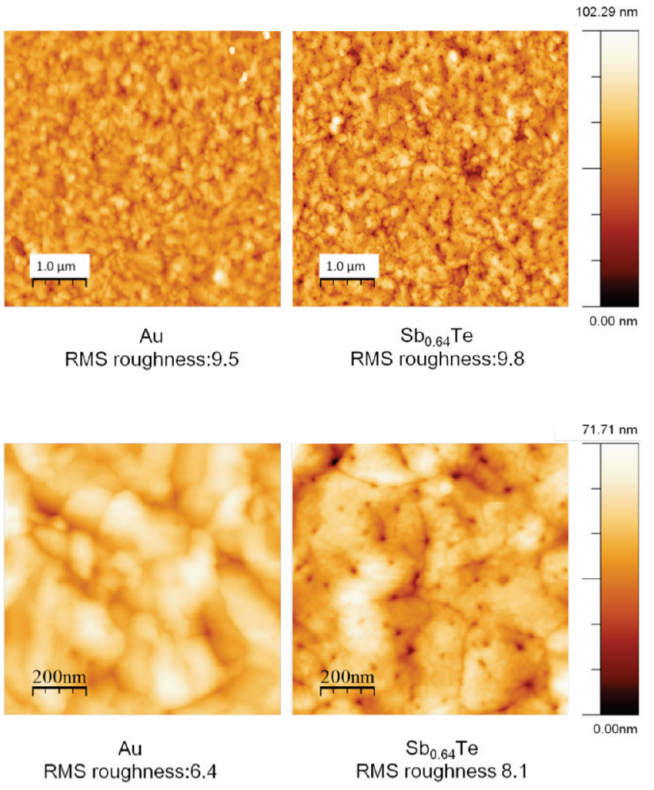

Figure 8. AFM images of a Au substrate and an as-deposited 100-cycle $Sb_{0.64}Te$ film deposited on a piece of the same Au substrate.

from 9% to about 0.3%, as the stripping potential shifted from −900 mV to −1150 mV (Figure 6). EPMA atomic % was calculated based on a homogeneous alloy model, rather than a Au substrate, with a thin film of Sb_xTe_y on top. The atomic % of Au was generally the largest. The atomic %, however, does give a roughly linear relation with coverage, for low atomic % elements. In Figure 6, the Sb % is seen to drop as well as that for Te, at lower potentials, although not as rapidly as the Te. The Sb % drops because Sb UPD only occurs on Te. Overall, the Sb/Te ratio (Figure 6) increased from 0.62 to 7.73, as the Te reductive stripping potential was changed from −900 mV to −1150 mV, though almost no Te was deposited as the potential approached −1150 mV. The Te stripping potential mediated Te stability on the surface, as positive potentials allowed less strongly held Te atoms to remain, whereas more negative Te stripping potentials left only the most stable Te.

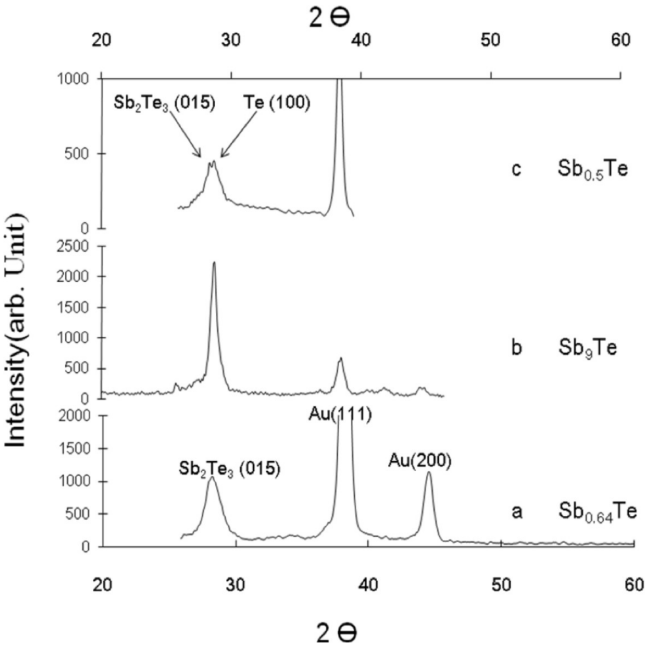

Figure 9. X-ray diffraction patterns of as deposited Sb_xTe_y films.

Figure 7 shows the composition as a function of the Sb deposition potential, while keeping the Te deposition potential at −700 mV and the stripping potential at −920 mV. The Sb UPD potential was changed from −740 to −650 mV. Clearly, the Sb and Te coverages follow each other, though the ratio of Sb/Te decreased as the potential for Sb UPD shifted positive. The positive shift, as expected, resulted in lower coverage Sb atomic layers. The Te coverage decreased with decreasing Sb, as there was less to bond with.

The above study of Sb_xTe_y deposition parameters resulted in conformal deposits, with Sb/Te ratios of from 10 to 0.45. The parameter space was: Te deposition potentials from −650 to −800 mV; Te reductive stripping potentials from −900 to −1150 mV, and Sb deposition potentials from −650 to −750 mV. Films made with those conditions showed no signs of roughening. Figure 8 displays AFM images for both a Au substrate and an as deposited $Sb_{0.64}Te$ film, formed with 100 cycles, on a piece of the same Au substrate. EPMA indicated a homogeneous distribution across the surface. Figure 9a displays an X-ray diffraction pattern for the as deposited $Sb_{0.64}Te$ film. The (015) peak for Sb_2Te_3, as well as the Au(111) and (200) are present.[17] An XRD pattern for a Sb rich deposit is shown in Figure 9b, for Sb_9Te. Pattern displays a convolution of peaks for Sb_2Te_3 and crystalline Sb, or possibly $Sb_{2n}Te_3$.[44] Figure 9c displays the XRD pattern of a $Sb_{0.5}Te$ film. It appears that Sb rich films were more readily formed than Te rich films. A small extra peak, possibly Te(100), showed up just above noise level, on the right side of the Sb_2Te_3(015) peak. Those XRD patterns were all recorded for as-deposited, unannealed Sb_xTe_y samples, and demonstrate how E-ALD tends to form more crystalline deposits than most other room temperature deposition processes, such as electrochemical codeposition.[19]

Ge_xTe_y. To this point, Ge_xTe_y has been synthesized using chemical vapor deposition,[45,46] but not electrodeposition. Development of an E-ALD cycle for the formation of Ge_xTe_y proceeded similarly to that for Sb_xTe_y. From Figures 1 and 3, the potentials needed to deposit Ge and Te are evident, as is that

dx.doi.org/10.1021/cm102672j |*Chem. Mater.* 2011, 23, 1742–1752

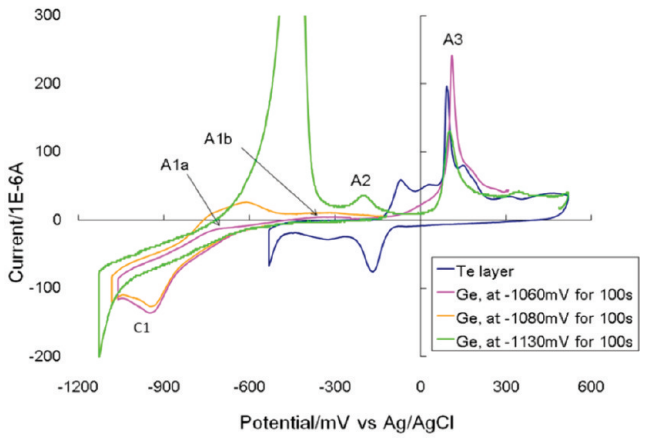

Figure 10. CVs of Te on Au (blue line) and Ge on the resulting Te layer, to different negative potential limits, where the potential was held for 100 s.

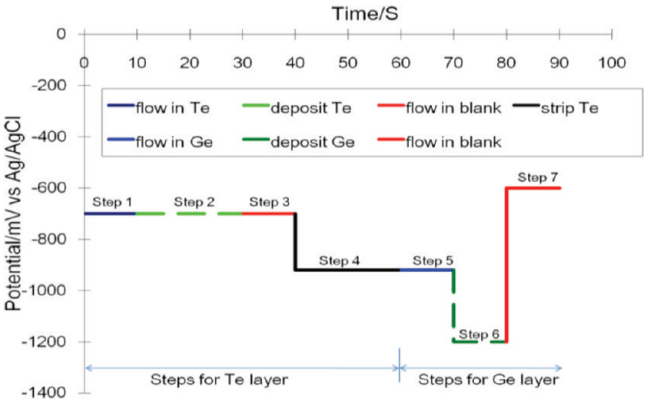

Figure 11. Example of a Ge_xTe_y deposition cycle. Solid lines indicate solution flowing and dashed lines indicate stagnant solutions.

needed to reduce Te to telluride. Solutions made using GeO_2 at pH 4.7, 9.4, and 11.85 were investigated with the intent of finding a Ge deposition potential positive of Te reductive stripping. However, both reactions are pH dependent, and their potentials shifted similarly with pH, Te reductive stripping always occurring positive of Ge deposition. The pH 9.4 showed the smallest potential difference.

Te and Ge deposition on each other had to be investigated in order to better understand the chemistry needed to design a Ge_xTe_y cycle. Figure 10 displays CVs for Te deposition (blue line) and Ge deposition on a Te covered Au substrates (pink, orange and green lines). The blue line (Figure 10) was deposition of the initial Te atomic layer. For the subsequent Ge deposition studies, the initial Te atomic layer was formed by scanning the Au substrate to −530 mV in the TeO_3^{2-} solution and then holding for 50 s. The resulting Te coverage was equivalent to the maximum surface limited Te coverage, plus about 0.2 ML of bulk, determined from coulometry during a subsequent oxidative scan, assuring a complete Te atomic layer on the Au surface.

After covering the surface with Te, the $HGeO_3^-$ solution was introduced and the substrate was scanned to different potentials for Ge deposition. The potential was held at the negative potential limit in each case for 100 s. The pink and orange scans are two examples of Ge deposition on a Te layer, and its subsequent stripping. In the initial negative going scan, peak C1 corresponded to reduction of weakly bound Te to Te^{2-}, leaving an atomic layer of more strongly bound Te. The increase in reductive current negative of C1 was due to the hydrogen evolution reaction (HER), Ge deposition, and reduction of a small amount of the strongly bound Te. The green line was a continuation of the orange line, after reversing at −150 mV. Note that no C1 feature was evident in the green line, as weakly bound Te had been stripped during the orange scan.

Attempts to deposit Ge at potentials positive of −1060 mV did not appear to work, as no Ge oxidation features (A1a or A1b) were evident in the positive going scan. However, deposition at −1080 mV, or negative, did result in oxidation features in the anodic scan, indicating Ge had deposited. The deposition potential for Ge on Te appears to have shifted negative by 250 mV, compared with Ge deposition on Au. Those results suggest a lower affinity of Ge for Te than Au, or slower Ge deposition kinetics on Te. As expected, the amounts of Ge deposited increased at more negative potentials (−1130 mV for the green line in Figure 10).

In the green line, positive of Ge stripping, the amount of Te stripping was down from the blue line, indicating that some Te was removed during Ge deposition. Te loss was evident from the decrease in A3, and indirectly, because of the increase in A2. A3 is oxidation of the Te atomic layer, and its decrease indicates loss of Te. The Te loss increases with decreasing potentials used for Ge deposition, suggesting Te was slowly reductively stripping during Ge deposition. Peak A2 has been observed in previous studies of Ge atomic layer formation on Au, and correspond to oxidation of a 4/9ths coverage Au(111)(3 × 3)-Ge atomic layer, observed via STM.[23] A2 is not evident in the pink and orange scans, as the Au surface was covered with Te. After scanning as far negative as −1130 mV (green line) A2 appears, however, indicating that some of the Te coating Au surface had been lost, and some Ge was present directly on the Au surface. That some of the Te was still present on the surface, as well, can be concluded from the presences of an A3 peak in the green line, though significantly diminished compared with the pink line. Apparently, by −300 mV, domains of Ge on Au and Te on Au exist simultaneously on the surface (green line).

As the dependence of Te atomic layer coverage has been discussed, with respect to the Te deposition potential and the Te reductive stripping potential, with regard to Ge_xTe_y formation, the discussion below will focus more on Ge deposition. Experiments were performed to study the effect of the Ge deposition potential on composition, by first forming a self-limited Ge layer, equivalent to about 3.5 ML,[23] on the Au surface. E-ALD of Ge_xTe_y was then performed on that surface, using a cycle consisting of one atomic layer of Te followed by one of Ge, and repeating (Figure 11). In Figure 11, as in Figure 4a, solid lines indicate flow while dashed lines indicate stagnant solutions. The cycle started by flowing TeO_3^{2-} solution through the cell for 10s at a fixed potential of −700 mV (step 1). In step 2, the potential was held for 20 s with the solution stagnant, allowing Te UPD and a small amount of bulk. In step 3, the blank was flowed for 10 s to remove excess TeO_3^{2-}, followed by stepping the potential to −920 mV to reductively strip bulk Te in the flowing blank (Step 4). In step 5, the $HGeO_3^-$ solution was flowed through for 10 s, still at −920 mV (step 5), followed by a potential step to −1200 mV for 10 s, without flowing (step 6), to

dx.doi.org/10.1021/cm102672j |Chem. Mater. 2011, 23, 1742–1752

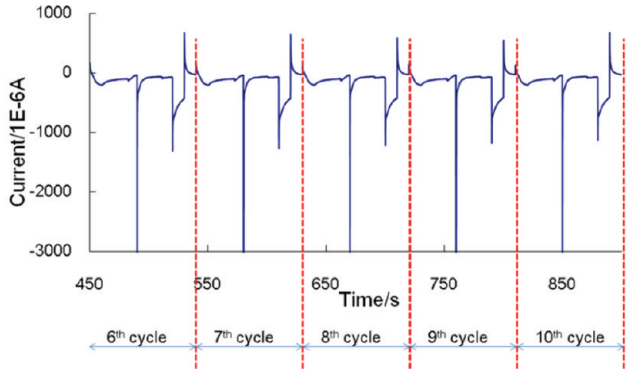

Figure 12. Current time curves for the 6th through 10th deposition cycles.

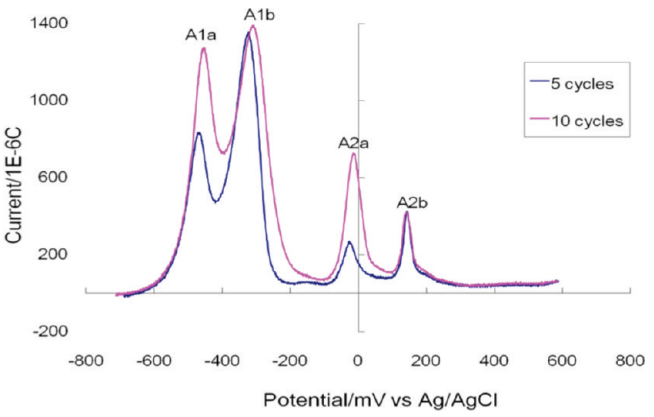

Figure 13. Oxidation of deposited Ge_xTe_y films.

deposit a Ge atomic layer. Step 7 was a blank flush, to remove excess $HGeO_3^-$ ions.

As previously report by this group, the amount of Ge that can be directly electrodeposited from an aqueous solution is self-limited, and a function of pH.[23] The maximum coverage at pH 9.4 was about 3.5 ML. In order to deposit more Ge, alternation with Te deposition, in a cycle, was required (Figure 11). The converse was true as well; Ge was required to prevent Te loss from reduction to Te^{2-} at the negative Ge deposition potentials. The potential range over which Ge deposition could be performed was thus limited. A reproducible cycle for Ge_xTe_y deposition was developed, as can be seen in Figure 12, where the current time traces for the sixth through 10th cycles are displayed.

Oxidation charges for stripping Ge and Te were used to determine the elemental composition of films formed using E-ALD cycles, for up to 10 cycles (Figure 13). There are four main peaks in Figure 13. Peaks A1a is oxidation of the top layer of Ge, and overlaps peak A1b, which is oxidiation of interior Ge, under Te. Peaks A2a is bulk Te oxidation, while A2b is oxidation of the last atomic layer of Te. Peak A1b is large, as it also contains the 3.5 ML of Ge, formed during the initial Ge reduction on the Au substrate, described above and in a previously article.[23] Thus, to study the composition of the Ge_xTe_y film formed using the E-ALD cycle, the difference between oxidation after fifth cycle and 10th cycle was determined (Figure 13), avoiding the contribution from the initial 3.5 ML deposit of Ge. The validity of Ge/Te ratios determined from the coulometry difference for

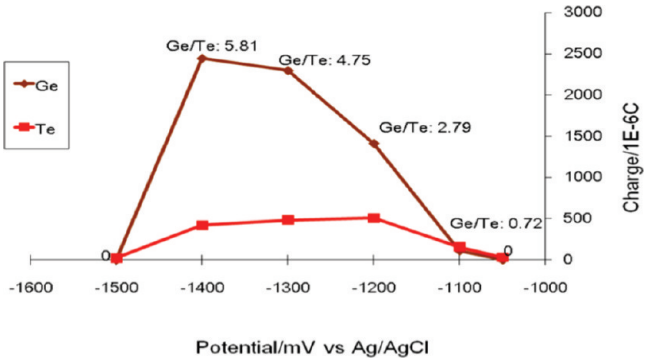

Figure 14. Ge and Te deposition amount per cycle as a function of Ge deposition.

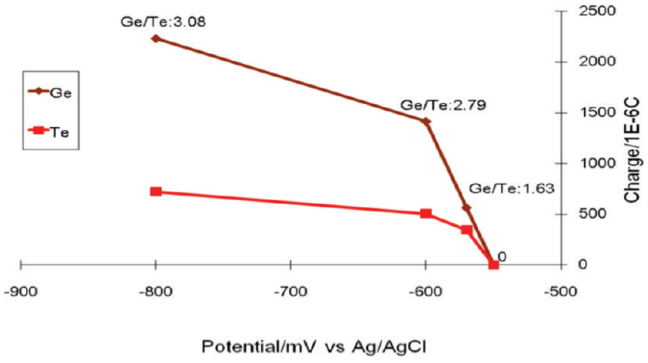

Figure 15. Amounts of Ge and Te deposition per cycle as a function of the Ge oxidative stripping potential (step 7 in Figure 11).

the fifth and 10th cycle deposits (Figure 13) was supported by equivalent results from EPMA of deposits formed with significantly more cycles.

Figure 14 shows how the Ge/Te ratio changed as a function of the Ge deposition potential (step 6 in Figure 11). At −1050 mV, the amounts of Ge and Te were both zero, as the potential was sufficiently positive that no Ge could deposit, and thus Te had no Ge to bind with. At a slightly more negative potential, −1100 mV, Ge was deposited, and so was Te, stabilized by the Ge, preventing its reductive stripping. The Ge/Te ratio (0.72) was low, as were the coverages of both elements. At −1200 mV, more Ge was deposited, though it became easier to reductively strip Te, so the Ge/Te ratio increased significantly. The same justifications can be applied to deposits formed using −1300 and −1400 mV, Ge deposition was more facile, as was Te reductive stripping, leading to further increases in the Ge/Te ratio (Figure 14). By −1500 mV, the potential was sufficiently negative, that all Te stripped, leaving none for Ge to deposit on.

Figure 15 shows how the Ge oxidative stripping potential can be used to adjust the deposition ratio. In that study, only the potential of Step 7 was changed, while the rest were kept as shown in Figure 11. As can be seen in Figure 13, Ge oxidation began around −700 mV, well below the −100 mV needed to oxidize Te. By using more positive potentials for the Ge oxidative stripping step, the Ge/Te ratio was lowered as only the Ge most stabilized by Te remained. By −550 mV, all the Ge was oxidized, and no deposit was formed (Figure 15).

The Ge_xTe_y nanofilms formed in these studies were smooth, and displayed Ge/Te ratios from 6 to 0.9, using deposition

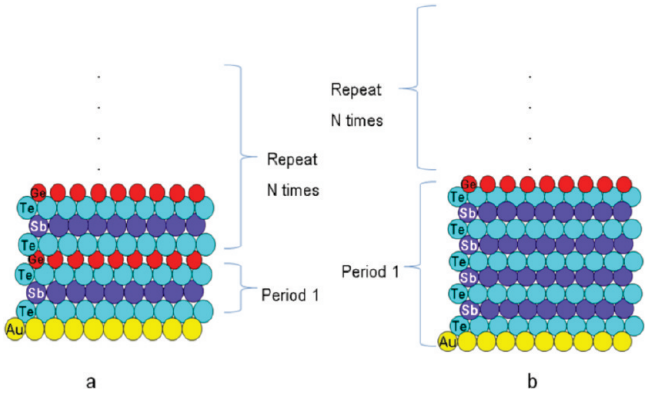

Figure 16. Schemes for two different $Ge_xSb_yTe_z$ superlattice programs (a) a $1Sb_xTe_y$:$1Ge_xTe_y$ and (b) a $4Sb_xTe_y$:$1Ge_xTe_y$.

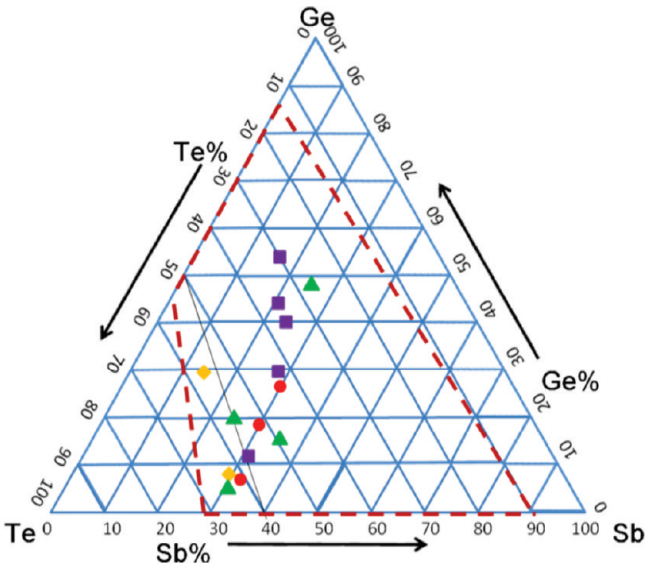

Figure 17. Dashed red line delineates the region over which the composition of $Ge_xSb_yTe_z$ appears adjustable using E-ALD and the superlattice program. Examples: red circles differ in the ratio of the # of cycles of Sb_xTe_y and Ge_xTe_y performed in the period; purple squares differ in the Ge deposition potential; yellow diamonds differ in the Ge deposition time; green triangles, random samples (Table 1).

conditions in the following ranges: Te deposition between −650 and −800 mV, Te reductive stripping between −900 and −1150 mV, Ge deposition between −1100 and −1400 mV, and Ge oxidative stripping between −700 and −570 mV. Ge deposition times were from 5 to 20 s.

$Ge_xSb_yTe_z$. Studies of the binary systems, Sb_xTe_y and Ge_xTe_y, demonstrated film compositions controllable over a wide range using E-ALD, with each cycle step representing a degree of control freedom over the deposit composition. All trends observed for control over composition of the binary films were maintained in the formation of the ternary system, $Ge_xSb_yTe_z$.

To form the ternary compound $Ge_xSb_yTe_z$, the binary cycle chemistries were combined using a "superlattice" program.[47,48] A superlattice is a structure composed of alternating nanofilms of two or more materials. By maintaining homogeneous nanofilm thicknesses from cycle to cycle, the deposit becomes periodic normal to the surface. A unique new lattice constant results, in

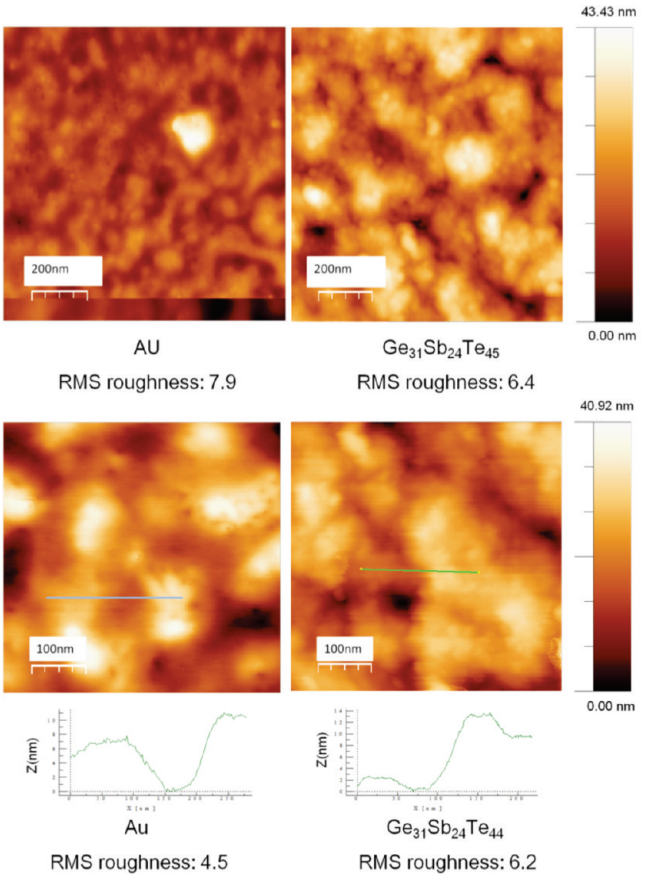

Figure 18. AFM images of a Au substrate and an as-deposited $Ge_{31}Sb_{24}Te_{45}$ film, deposited on the substrate.

essences producing a new material.[31,49−52] The E-ALD software being used allowed superlattice formation with a variety of periods. The period describes how the superlattice was formed. In the present study, the period was the sum of the number of Sb_xTe_y cycles, together with the number of Ge_xTe_y cycles performed. Each period can then be repeated, with the number of repetitions determining the deposit thickness. The simplest superlattice program was one cycle of each (Figure 16a), a $1Sb_xTe_y$:$1Ge_xTe_y$ period. Figure 16b displays a $4Sb_xTe_y$:$1Ge_xTe_y$ period, designed to decrease the amount of Ge in the deposit.

Figure 17 is a ternary phase diagram for $Ge_xSb_yTe_z$, displaying deposit compositions achieved using a variety of different E-ALD period programs. Red dots are deposits where the cycle programs for Sb_xTe_y and Ge_xTe_y were held constant, and only the relative numbers of cycles for each in a period were changes. Red dots from left to right display a decreasing Te percent. The left red dot was grown using a 5:1 period of Sb_xTe_y and Ge_xTe_y cycles, the middle was a 3:1, and the right (top) dot was a 2:1 period. The atomic % of Ge was systematically increased, and that for Te decreased, by decreasing the number of Sb_xTe_y cycles per period. The systematic decrease in Te atomic % resulted from the higher proportion of % of Ge_xTe_y cycles, where some Te reduced away during Ge deposition, as described for Ge_xTe_y formation above.

The purple squares (Figure 17) were a function of the Ge deposition potential. All were formed using a 2:1 period of Sb_xTe_y and Ge_xTe_y. All parameters were constant except the Ge deposition potential. From the top to the bottom, the atomic % of Ge decreased as the deposition potential increased (−1250 to

dx.doi.org/10.1021/cm102672j |*Chem. Mater.* 2011, 23, 1742–1752

Table 1. Main Deposition Parameters for the Green Triangles in Figure [17,a]

	period of Sb_xTe_y:Ge_xTe_y	Te deposition potential mV	Te stripping potential mV	Sb deposition Potential mV	Ge deposition Potential mV	Ge deposition Time s	Ge oxidative stripping potential mV
1	5:5	−700	−910	−680	−1100	3	−910
2	2:1	−700	−920	−720	−1200	5	−620
3	2:1	−720	−950	−680	−1200	5	−620
4	5:5	−700	−910	−680	−1120	10	−910
5	2:1	−720	−950	−720	−1250	5	−660

[a] 1 is the bottom green triangle, which has the lowest Ge amount, and 5 is the top green triangle, which has the highest Ge amount. The times for Te deposition, Te stripping and Sb deposition are all 20s and the times can be used variables too.

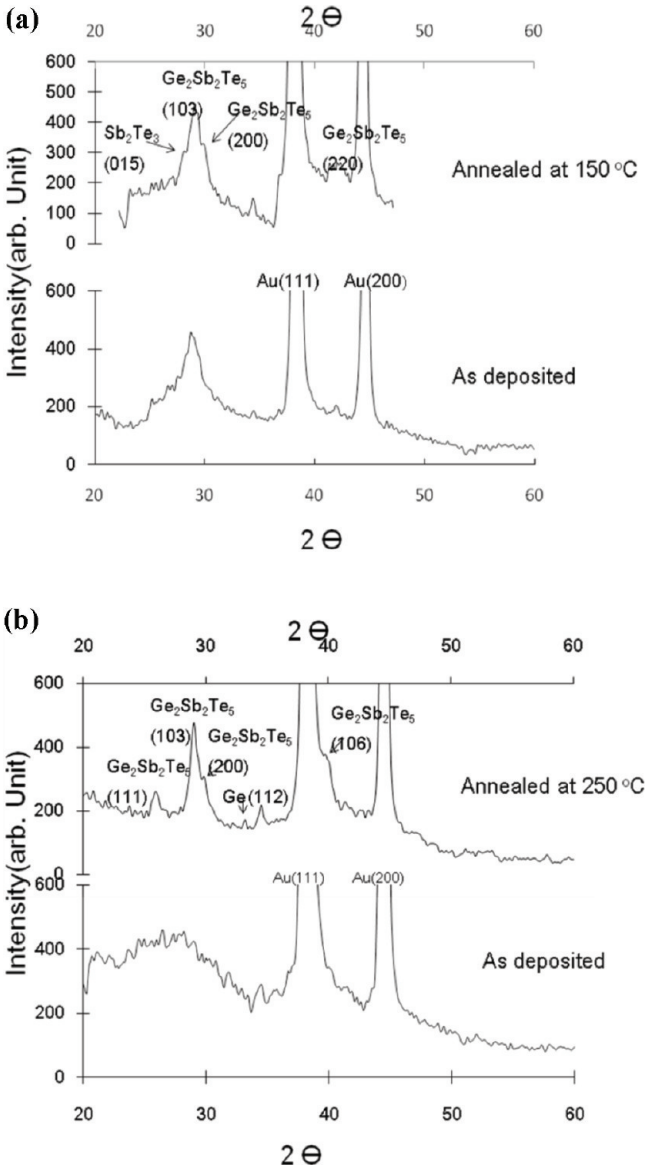

Figure 19. (a) X-ray diffraction patterns of a $Ge_{20}Sb_{32}Te_{48}$ film, before and after annealing. (b) X-ray diffraction patterns of $Ge_{31}Sb_{24}Te_{45}$ film before and after annealing.

−1120 mV). The orange diamond deposits (Figure 17) were grown with a 5:5 period, with the only variable being the time for Ge deposition. The upper diamond used 20s and the lower was 5s for Ge deposition. Clearly the Ge deposition step was not a fully surface limited reaction. The deposit lower in Ge was also higher in Te, than the upper orange diamond. As noted above, in the discussions of Ge_xTe_y formation, the Ge deposition potential was negative enough for Te reductive stripping, therefore the less time for Ge deposition, the less time to reductively strip Te. Overall, the step appears to be controlled by the kinetics for Ge deposition and Te stripping. To keep the Ge coverage up, a period including more Ge_xTe_y cycles and longer Ge deposition times should be used. To increase the Te coverage, more positive Ge deposition potentials would keep Te reductive stripping down and its coverage up. Te on the exterior of the Sb_xTe_y nanofilms, could be reductively stripped, as well, during Ge deposition. Extra cycles of Sb_xTe_y each period might help protect Te from stripping. The green triangles in Figure 17 were from films formed using a variety of other conditions (Table 1). Conditions were sought that would result in deposits high in Te and Ge, as deposits high in Sb were relatively easy to achieve.[32] The binary Sb_xTe_y can be made with a Sb/Te ratio ranging from 10 to 0.45, whereas Ge_xTe_y can be made within a Ge/Te ratio ranging from 6 to 0.9. Theoretically, deposits anywhere within the red dashed region of Figure 17 can be formed.

No sign of roughening was observed for the films grown for the construction of Figure 17. Figure 18 displays AFM images of a Au substrate and an as deposited 100 cycle $Ge_{31}Sb_{24}Te_{45}$ film. X-ray data suggests that the films were more crystalline, the less Ge they contained. Figure 19a (lower pattern) displays a glancing incidence X-ray diffraction pattern for an as deposited $Ge_{20}Sb_{32}Te_{48}$ film. The broad peak near 29° is probably overlap of peaks for several similar compounds. Vapor deposition has normally resulted in a large bump around 29°, as well.[10,14,19,53] After the sample was annealed at 150 °C for 20 min in nitrogen, the peak shifted slightly to the right and became a little more defined. Possible stoichiometries responsible for the features are noted in Figure 19. For films with a higher Ge atomic %, $Ge_{31}Sb_{24}Te_{45}$ for example (Figure 19b), as deposited they did not display a peak, just a large bump. Annealing to 250 °C for 20 min in nitrogen resulted in the resolution of several peaks, and possible stoichiometries were again noted (Figure 19b).

CONCLUSION

The phase change material $Ge_xSb_yTe_z$ was conformally deposited using electrochemical atomic layer deposition (E-ALD). These results showed wide latitude in the deposit compositions formed, including those desirable for memory applications. Deposition parameters and applicable potential ranges included: Te deposition from −650 to −800 mV, Te reductive stripping from −900 to −1150 mV, Ge deposition from −1100 to −1400 mV,

dx.doi.org/10.1021/cm102672j |Chem. Mater. 2011, 23, 1742–1752

Ge oxidative stripping from −700 to −570 mV, and Sb deposition from −650 to −750 mV. Changing the deposition conditions for one element generally had a secondary, though predictable, effect on another. pH 9.4 was selected for $Ge_xSb_yTe_z$ deposition because it minimized issues between Ge deposition and Te reductive stripping.

E-ALD tends to form deposits with better crystallinity than those formed by vapor deposition or electrochemical codeposition, at room temperature.[10,14,17,19,53] Advantages of E-ALD include room temperature and ambient pressure growth, and use of simple low concentration aqueous solutions. ALD in general provides atomic level control over deposit thickness, and conformal deposition. In addition, E-ALD affords numerous parameters for optimization and the low cost of an electrochemical process, making it a promising nanofilms deposition methodology.

AUTHOR INFORMATION

Corresponding Author

*E-mail: stickney@chem.uga.edu.

ACKNOWLEDGMENT

Acknowledgment is made to the National Science Foundation, Division of Materials, for its support.

REFERENCES

(1) Wuttig, M.; Yamada, N. *Nat. Mater.* **2007**, *6* (12), 1004–1004.
(2) Raoux, S. *Ann. Rev. Mater. Res.* **2009**, *39* (1), 25–48.
(3) Kolobov, A. V.; Fons, P.; Frenkel, A. I.; Ankudinov, A. L.; Tominaga, J.; Uruga, T. *Nat. Mater.* **2004**, *3* (10), 703–708.
(4) Redaelli, A.; Pirovano, A.; Pellizzer, E.; Lacaita, A. L.; Ielmini, D.; Bez, R. *IEEE Electron Device Lett.* **2004**, *25* (10), 684–686.
(5) Raoux, S.; Shelby, R. M.; Jordan-Sweet, J.; Munoz, B.; Salinga, M.; Chen, Y.-C.; Shih, Y.-H.; Lai, E.-K.; Lee, M.-H. *Microelectron. Eng.* **2008**, *85* (12), 2330–2333.
(6) Welnic, W.; Wuttig, M. *Mater. Today* **2008**, *11* (6), 20–27.
(7) Raoux, S.; Wełnic, W.; Ielmini, D. *Chem. Rev.* **2009**, *110* (1), 240–267.
(8) Welnic, W.; Pamungkas, A.; Detemple, R.; Steimer, C.; Blugel, S.; Wuttig, M. *Nat. Mater.* **2006**, *5* (1), 56–62.
(9) Yamada, N.; Ohno, E.; Nishiuchi, K.; Akahira, N.; Takao, M. *J. Appl. Phys.* **1991**, *69* (5), 2849–2856.
(10) Prikryl, J.; Hrdlicka, M.; Frumar, M.; Orava, J.; Benes, L.; Vlcek, M.; Kostal, P.; Hromadko, L.; Wagner, T. *J. Non-Cryst. Solids* **2009**, *355* (37−42), 1998–2002.
(11) Reifenberg, J. P.; Panzer, M. A.; Kim, S.; Gibby, A. M.; Zhang, Y.; Wong, S.; Wong, H. S. P.; Pop, E.; Goodson, K. E. *Appl. Phys. Lett.* **2007**, *91* (11), 3.
(12) Sun, Z.; Kyrsta, S.; Music, D.; Ahuja, R.; Schneider, J. M. *Solid State Commun.* **2007**, *143* (4−5), 240–244.
(13) Choi, B. J.; Choi, S.; Shin, Y. C.; Hwang, C. S.; Lee, J. W.; Jeong, J.; Kim, Y. J.; Hwang, S.-Y.; Hong, S. K. *J. Electrochem. Soc.* **2007**, *154* (4), H318–H324.
(14) Kim, R. Y.; Kim, H. G.; Yoon, S. G. *Appl. Phys. Lett.* **2006**, *89*, 10.
(15) Lee, J.; Choi, S.; Lee, C.; Kang, Y.; Kim, D. *Appl. Surf. Sci.* **2007**, *253* (8), 3969–3976.
(16) Milliron, D. J.; Raoux, S.; Shelby, R.; Jordan-Sweet, J. *Nat. Mater.* **2007**, *6* (5), 352–356.
(17) Venkatasamy, V.; Shao, I.; Huang, Q.; Stickney, J. L. *J. Electrochem. Soc.* **2008**, *155* (11), D693–D698.
(18) Shao, X. H., Q. ; Stickney J. L.; Venkatasamy, V., , U.S. Patent Appl. No. 20090011577.
(19) Huang, Q.; Kellock, A. J.; Raoux, S. *J. Electrochem. Soc.* **2008**, *155* (2), D104–D109.
(20) Panicker, M. P. R.; Knaster, M.; Kroger, F. A. *J. Electrochem. Soc.* **1978**, *125* (4), 566–572.
(21) Kroger, F. A. *J. Electrochem. Soc.* **1978**, *125* (12), 2028–2034.
(22) Erdogan, I. Y.; Demir, Ü. *J. Electroanal. Chem.* **2009**, *633* (1), 253–258.
(23) Liang, X.; Kim, Y.-G.; Gebergziabiher, D. K.; Stickney, J. L. *Langmuir* **2009**, *26* (4), 2877–2884.
(24) Thambidurai, C.; Gebregziabiher, D. K.; Liang, X. H.; Zhang, Q. H.; Ivanova, V.; Haumesser, P. H.; Stickney, J. L. *J. Electrochem. Soc.* **2010**, *157* (8), D466–D471.
(25) Leimkuhler, G.; Kerkamm, I.; Reineke-Koch, R. *J. Electrochem. Soc.* **2002**, *149* (10), C474–C478.
(26) Pirovano, A.; Pellizzer, F.; Tortorelli, I.; Rigan, A.; Harrigan, R.; Magistretti, M.; Petruzza, P.; Varesi, E.; Redaelli, A.; Erbetta, D.; Marangon, T.; Bedeschi, F.; Fackenthal, R.; Atwood, G.; Bez, R. *Solid-State Electron.* **2008**, *52* (9), 1467–1472.
(27) Shin, J. M.; Song, Y. J.; Kang, D. W.; Jeong, C. W.; Ryoo, K. C.; Park, J. H.; Oh, J. H.; Kong, J. H.; Jae; Park; Fai, Y.; Oh, Y. T.; Kim, J. I.; Lim, D. W.; Park, S.; Kim, J. H.; Kim, J. S.; Kim, Y. T.; Koh, G. H.; Jeong, G. T.; Jeong, H. S.; Kim, K. *Integr. Ferroelectr.* **2007**, *90*, 88–+.
(28) Banga, D. O.; Vaidyanathan, R.; Liang, X. H.; Stickney, J. L.; Cox, S.; Happeck, U. *Electrochim. Acta* **2008**, *53* (23), 6988–6994.
(29) Thambidurai, C.; Kim, Y. G.; Jayaraju, N.; Venkatasamy, V.; Stickney, J. L. *J. Electrochem. Soc.* **2009**, *156* (8), D261–D268.
(30) Kim, Y.-G.; Kim, J. Y.; Thambidurai, C.; Stickney, J. L. *Langmuir* **2007**, *23* (5), 2539–2545.
(31) Vaidyanathan, R.; Cox, S. M.; Happek, U.; Banga, D.; Mathe, M. K.; Stickney, J. L. *Langmuir* **2006**, *22* (25), 10590–10595.
(32) Shao, X. H., Q. ; Kellock A. J. ; Venkatasamy, V., , U.S. Patent Appl. No. 20090071836, .
(33) Flowers, B. H.; Wade, T. L.; Garvey, J. W.; Lay, M.; Happek, U.; Stickney, J. L. *J. Electroanal. Chem.* **2002**, *524−525*, 273–285.
(34) Yan, J. W.; Wu, Q.; Shang, W. H.; Mao, B. W. *Electrochem. Commun.* **2004**, *6* (8), 843–848.
(35) Hara, M.; Inukai, J.; Yoshimoto, S.; Itaya, K. *J. Phys. Chem. B* **2004**, *108* (45), 17441–17447.
(36) Li, F. H.; Wang, W.; Gao, J. P.; Wang, S. Y. *J. Electrochem. Soc.* **2009**, *156* (3), D84–D91.
(37) Sorenson, T. A.; Varazo, K.; Suggs, D. W.; Stickney, J. L. *Surf. Sci.* **2001**, *470* (3), 197–214.
(38) Gregory, B. W.; Suggs, D. W.; Stickney, J. L. *J. Electrochem. Soc.* **1991**, *138* (5), 1279–1284.
(39) Varazo, K.; Lay, M. D.; Sorenson, T. A.; Stickney, J. L. *J. Electroanal. Chem.* **2002**, *522* (1), 104–114.
(40) Lay, M. D.; Stickney, J. L. *J. Electrochem. Soc.* **2004**, *151* (6), C431–C435.
(41) Yang, J. Y.; Zhu, W.; Gao, X. H.; Fan, X. A.; Bao, S. Q.; Duan, X. K. *Electrochim. Acta* **2007**, *52* (9), 3035–3039.
(42) Park, K.; Xiao, F.; Yoo, B. Y.; Rheem, Y.; Myung, N. V. *J. Alloys Compd.* **2009**, *485* (1−2), 362–366.
(43) Yang, J.; Zhu, W.; Gao, X.; Bao, S.; Fan, X.; Duan, X.; Hou, J. *J. Phys. Chem. B* **2006**, *110* (10), 4599–4604.
(44) Prokhorov, E.; Gonzalez-Hernandez, J.; Hernandez-Landaverde, M. A.; Chao, B.; Morales-Sanchez, E. *J. Phys. Chem. Solids* **2007**, *68* (5−6), 883–886.
(45) Kim, R. Y.; Kim, H. G.; Yoon, S. G. *J. Electrochem. Soc.* **2008**, *155* (2), D137–D140.
(46) Abrutis, A.; Plausinaitiene, V.; Skapas, M.; Wiemer, C.; Gawelda, W.; Siegel, J.; Rushworth, S. *J. Cryst. Growth* **2009**, *311* (2), 362–367.
(47) Venkatasamy, V.; Jayaraju, N.; Cox, S. M.; Thambidurai, C.; Stickney, J. L. *J. Electrochem. Soc.* **2007**, *154* (8), H720–H725.
(48) Loglio, F.; Innocenti, M.; Pezzatini, G.; Foresti, M. L. *J. Electroanal. Chem.* **2004**, *562* (1), 117–125.
(49) Switzer, J. A.; Shane, M. J.; Phillips, R. J. *Science* **1990**, *247* (4941), 444–446.

(50) Phillips, R. J.; Golden, T. D.; Shumsky, M. G.; Bohannan, E. W.; Switzer, J. A. *Chem. Mater.* **1997**, *9* (7), 1670–1677.
(51) Kothari, H. M.; Vertegel, A. A.; Bohannan, E. W.; Switzer, J. A. *Chem. Mater.* **2002**, *14* (6), 2750–2756.
(52) Switzer, J. A.; Gudavarthy, R. V.; Kulp, E. A.; Mu, G.; He, Z.; Wessel, A. J. *J. Am. Chem. Soc.* **2010**, *132* (4), 1258–1260.
(53) Kyrsta, S.; Cremer, R.; Neuschütz, D.; Laurenzis, M.; Haring Bolivar, P.; Kurz, H. *Appl. Surf. Sci.* **2001**, *179* (1−4), 55–60.